Deblended-data Reconstruction Using Generalized Blending and Deblending Models

Ishiyama, T; Ishikawa, S.; Ali, M; Nakayama, Shotaro; Blacquière, Gerrit

DOI
10.3997/2214-4609.201801535

Publication date
2018

Document Version
Final published version

Published in
80th EAGE Conference and Exhibition 2018, 11-14 June, Copenhagen, Denmark

Th P1 07

Deblended-data Reconstruction Using Generalized Blending and Deblending Models

T. Ishiyama* (Khalifa University of Technology), S. Ishikawa (Khalifa University of Technology), M. Ali (Khalifa University of Technology), S. Nakayama (Delft University of Technology), G. Blacquiere (Delft University of Technology)

Summary

We introduce a generalized concept of blending and deblending, and establish the generalized-blending and -deblending models. Accordingly, we establish a method of deblending, or deblended-data reconstruction, using these models.

The generalized blending can handle real-life situations; this includes random encoding both in the space and time domain, both at the source and receiver side, thus all incoherent and inhomogeneous shooting, signature stamping, non-uniform and under sampling. Similarly, the generalized deblending includes data reconstruction that works all for shot-generated-wavefields separation, spectrum recovery and balancing, designature, regularization and interpolation, again both at the source and receiver side. However, we do face a challenging question: how to fully reconstruct deblended data from the fully generalized blended data. To address this, we consider an iterative optimization scheme using a so-called closed-loop approach with the generalized-blending and -deblending models, in which the former works for the forward modelling and the latter for the inverse modelling in the closed loop. We established and applied this method to synthetic datasets. The results show that our method succeeded to fully reconstruct deblended data from the fully generalized blended data.

Introduction

In traditional acquisition, spatial and temporal interference between shots is avoided, often resulting in poor sampling in the source dimension. However, in blended acquisition, the interference is allowed, leading to dense and wide sampling in an economical way. We can achieve this by blending and deblending, i.e. blended acquisition followed by deblended-data-reconstruction processing.

As for blending at the source side, first, blended acquisition stands for continuous recording of seismic responses from incoherent shooting, the properties of which are characterized and encoded by random spatial distribution and time shifts among the involved source units of blended-source array (Berkhout, 2008). Second, blended acquisition uses inhomogeneous shooting, in which the blended-source array consists of different source units rather than traditional equal ones, e.g. narrow-frequency-banded versions instead of a certain broad-frequency-band one: dispersed source array, or DSA (Berkhout, 2012). Third, this acquisition also uses signature stamping, in which each source unit is encoded with its own signature, e.g. various sweeping for land (Bagaini, 2006); popcorn shooting for marine (Abma and Ross, 2013). Furthermore, another concept, particularly at the receiver side, is spatial sampling based on compressive sensing, which adopts non-uniform- and under-sampling acquisition followed by regularization and interpolation processing; where a signal can be recovered from far fewer samples than required by the Shannon-Nyquist theorem (Mosher et al., 2014).

In this paper, we introduce a generalized concept of blending and deblending, and establish the generalized-blending and -deblending models including all the above manners. Accordingly, we establish a method of deblended-data reconstruction using these models.

Generalized blending and deblending

For real-life situations, we can build a generalized concept of blending, which includes random encoding both in the space and time domain, both at the source and receiver side, thus all the above-mentioned means. In fact, incoherent and inhomogeneous shooting and signature stamping are special cases of blending only at the source side; non-uniform and under sampling are special cases of blending with randomizing only in the space domain. Similarly, a generalized concept of deblending includes data reconstruction that can work all for shot-generated-wavefields separation, spectrum recovery and balancing, designature, regularization and interpolation, again both at the source and receiver side.

For these generalized concepts, we do face a challenging question: how to fully reconstruct deblended data from the fully generalized blended data. To address this, we consider an iterative optimization algorithm using a so-called closed-loop approach. We use the properties of blended signal introduced by blending codes that contain shot locations, times, signatures, etc. of the involved source units of blended-source array. One of the properties is the coherency of blended signal versus the incoherency of blending noise in the pseudo-deblended domain, i.e. the domain after the adjoint of blending operation has been applied. This can be posed as an inverse problem with quantifying the coherency and its solutions by selecting optimal metrics of the coherency.

Theory and method

To describe seismic data, we introduce the so-called WRW model. In this model, seismic events can be described for each monochromatic component by operator matrices. Each matrix multiplication represents a multi-dimensional spatial convolution, and each element of every matrix contains amplitude and phase information. Using this representation, we can describe a forward model as:

$$\mathbf{P}'' = \mathbf{\Gamma}_D \mathbf{P} \mathbf{\Gamma}_S, \quad (1)$$

$$\mathbf{P} = \mathbf{L}^H \mathbf{M}, \quad (2)$$

where $\mathbf{P}''$ is the blended data on an observed grid, $\mathbf{P}$ is the unblended data on a nominal grid, both in the measurement domain (e.g. the space-time domain). $\mathbf{\Gamma}_S$ and $\mathbf{\Gamma}_D$ are the generalized-blending operators, i.e. the generalized-shooting operator at the source side and the generalized-sensing operator at the receiver side. The forward model corresponds to the generalized-blending operation. This can include random encoding both in the space and time domain, containing the locations, times, signatures, etc., thus all incoherent and inhomogeneous shooting, signature stamping, non-uniform and under sampling, each at the source and receiver side. Incoherent and inhomogeneous sensing can

also be included theoretically at the receiver side, but might not be practical in real-life situations. **M** is the data in a transform domain (e.g. the Fourier domain). **L** is the transform operator, and $\mathbf{L}^H$ is the adjoint of **L** where the superscript $\blacksquare^H$ denotes Hermitian, i.e. conjugate transpose. Similarly, we can describe an inverse model as:

$$\mathbf{\Gamma}_D{}^H\mathbf{P}''\mathbf{\Gamma}_S{}^H = \mathbf{P}, \quad (3)$$

$$\mathbf{LP} = \mathbf{M}. \quad (4)$$

The inverse model corresponds to the generalized-deblending operation. This is data reconstruction that can include all shot-generated-wavefields separation, spectrum recovery and balancing, designature, regularization and interpolation again each at the source and receiver side. In these models, the blended data for a basis function, **P**'', is parameterized by the samples in the transform domain, **M**.

Given these models and the observed data, **P**'', our goal is then to solve for the model parameters, **M**, and the reconstructed data, **P**(**M**). We can describe the inverse problem as minimizing the objective function:

$$J = ||\mathbf{P}'' - <\mathbf{P}''>||^2 \text{ is minimum}, \quad (5)$$

where the angle brackets <▪> denote 'estimated'. For instance, if certain samples in the transform domain, <**M**>, are the solution in Equation 5, $<\mathbf{P}_M> = \mathbf{L}^H <\mathbf{M}>$ is the deblended data on the nominal grid, and then $<\mathbf{P}''> = \mathbf{\Gamma}_D<\mathbf{P}_M>\mathbf{\Gamma}_S$ is the reblended data on the observed grid in the measurement domain. The spatial sampling intervals and apertures of the nominal grid can be arbitrary determined.

To solve the inverse problem, we introduce a closed-loop approach. Figure 1 illustrates the conceptual flow. The closed loop contains not only the inversion module (steps in blue in the figure) but also the forward-modelling module (steps in red in the figure), allowing evaluation of the residual between observed and estimated data, $\Delta\mathbf{P}'' = \mathbf{P}'' - <\mathbf{P}''>$, thus feedback from the estimated model parameters, <**M**>, via the estimated data, <**P**''>. The model parameters can be iteratively estimated and selected under sparsity constraints such that the estimated data match the observed data, thus the residual is minimized.

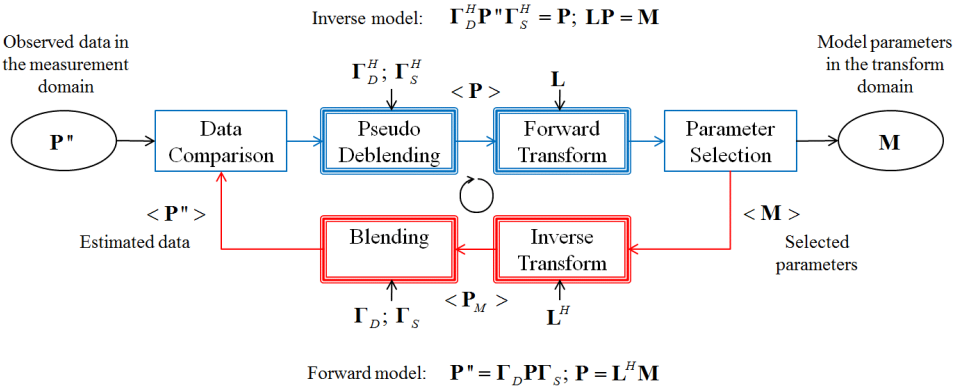

Figure 1 *Conceptual flow of the closed-loop approach for deblended-data reconstruction.*

For our closed-loop approach of deblended-data reconstruction, the transform domain is a 3-D Fourier domain, or more specifically the k_Dk_S-f domain, where k_D and k_S represent the wavenumbers each in the receiver and source dimension, and f for the frequency. The blended signal is more sparsely compressed in this domain, rather than in a conventional Fourier domain. For each iteration, the model parameters are selected by coherency-pass filtering in this domain followed by thresholding in the space-time domain. The estimate is updated by applying a scale to the gradient of objective function and adding it to the previous estimate so that the residual can be oriented to the minimum.

Examples

We demonstrate our method of deblended-data reconstruction with 2-D synthetic-data examples. First, traditional unblended data, **P**, were simulated from Marmousi model. The number of shot points is 100, and 100 for receiver points as well. The spatial sampling intervals and apertures are 10 m and

1000 m, respectively, both for the sources and receivers. Then, blended data, **P**'', were numerically synthesized with several blending scenarios. The blending fold, i.e. the number of involved source units in blended-source array, is 2. The maximum spatial separation is 500 m, and the maximum random time shift is 0.256 sec. The blending scenarios, represented by generalized-blending operators $\mathbf{\Gamma}_S$ and $\mathbf{\Gamma}_D$ for each case, are as follows:

1. Incoherent shooting only at the source side.

For marine,

2. Inhomogeneous shooting at the source side in addition to the scenario 1, by using 3 frequency-banded airgun units in marine DSA: low-frequency-banded unit of 4-12 Hz; mid of 16-24 Hz; high of 32-96 Hz, with random spatial distribution and multi-scale spatial sampling: 11 % of 100 shot points for low; 22 % for mid; 67 % for high.
3. Self-inhomogeneous, or popcorn shooting at the source side in addition to the scenario 1, by using 3 frequency-banded airgun units in marine popcorn-shooting array: low-frequency-banded unit of 4-12 Hz; mid of 16-24 Hz; high of 32-96 Hz, with random and multi-scale shot repetition at each shot point: 1 of 9 repetitions for low; 2 for mid; 6 for high.

For land,

4. Inhomogeneous sweeping at the source side in addition to the scenario 1, by using 3 frequency-banded vibroseis units in land DSA with the array configuration same as for the scenario 2.

For transition-zone (TZ),

5. Fully generalized case with the scenarios 1, 2 and 4, with random spatial distribution: 50 % of 100 shot points for marine DSA; 50 % for land DSA. In addition, non-uniform and under sampling both at the source and receiver side, by applying 9 % random decimation each at the source and receiver side, consequently about 25 % in total.

The sequent figures show five examples with the blending scenarios 1 to 5, respectively, followed by deblended-data reconstruction. Figure 2 shows the first example. The first row shows the inputs including the blended data, **P**'', in the common-source (and -receiver) domain. For the pseudo-deblended data, $\mathbf{P}_P$, the blended signal is coherent but the blending noise is incoherent in the common-receiver domain, indicating that the coherency is effectively promoted in this domain. The second row shows the outputs including the deblended data, $\langle\mathbf{P}\rangle$, after 100 iterations. In addition to the residual between blended and reblended data, $\Delta\mathbf{P}'' = \mathbf{P}'' - \langle\mathbf{P}''\rangle$, the difference between unblended and deblended data, $\Delta\mathbf{P} = \mathbf{P} - \langle\mathbf{P}\rangle$, can be displayed since the unblended data, **P**, are known here. This also makes it possible to estimate the S/N, $\mathbf{P}/\Delta\mathbf{P}$, besides the residual, $\Delta\mathbf{P}''/\mathbf{P}''$. The residual significantly improved 66 dB down and the S/N consequently rose 34 dB up. This demonstrates that our method successfully reconstructed the deblended data from the blended data, in particular separated the interfered shot-generated wavefields very well.

Figure 3 shows the other examples. The blended data, **P**'', at the top and the deblended data, $\langle\mathbf{P}\rangle$, after 100 iterations with the S/N value at the bottom; see Figure 2a for comparison with the unblended data, **P**. The examples 2 and 4 (Figures 3a and 3c) indicate that our method well reconstructed the full-frequency-band deblended data from the blended data shot by the narrow-frequency-banded source units in DSA, thus it entirely recovered and balanced the temporal spectrum. Moreover, the examples 3 and 4 (Figures 3b and 3c) indicate that our method properly reconstructed the designatured deblended data from the signature-stamped blended data. Furthermore, the example 5 (Figure 3d) reveals that our method nicely reconstructed the regularized and interpolated blended data from the non-uniform- and under-sampled blended data. For the example 5, the residual resulted in 69 dB down and the S/N in 24 dB up. The S/N value is lower than the others, indicating that more complicated blending situations negatively affect the resulting deblending performance. Nevertheless, the S/N value is quite acceptable in general in seismic processing. This demonstrates that our method fully reconstructed the deblended data from the fully generalized blended data quite well, thus it totally and simultaneously achieved all shot-generated-wavefields separation, spectrum recovery and balancing, designature, regularization and interpolation both at the source and receiver side.

Conclusions

We established generalized-blending and -deblending models and a method of deblended-data reconstruction using these models. Our methodology is quite practical, and can handle real-life

situations, such as: incoherent and inhomogeneous shooting, signature stamping, non-uniform and under sampling both at the source and receiver side for generalized blending; shot-generated-wavefields separation, spectrum recovery and balancing, designature, regularization and interpolation again both at the source and receiver side for generalized deblending. Our method of deblended-data reconstruction succeeded to fully reconstruct deblended data from the fully generalized blended data.

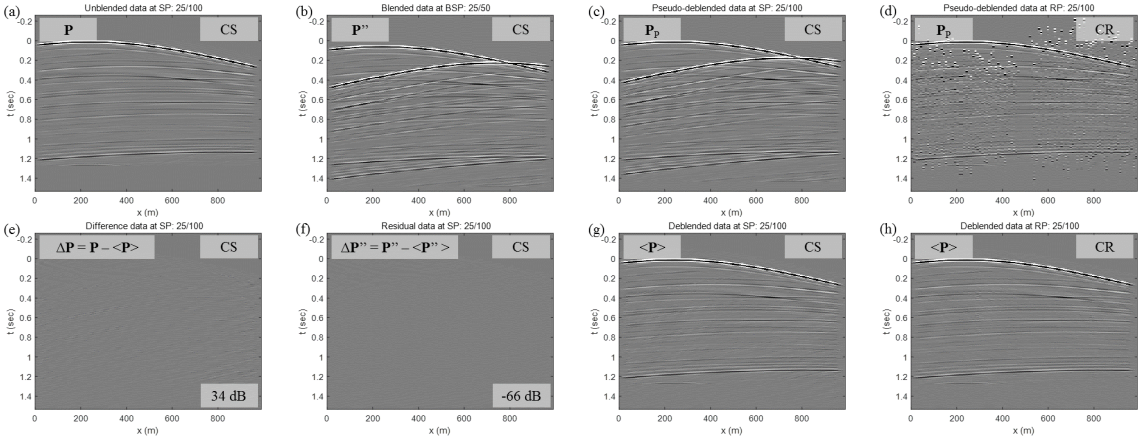

Figure 2 *Results for the blending scenario 1. Inputs: (a) unblended data; (b) blended data; (c) and (d) pseudo-deblended data in the common-source (CS) and -receiver (CR) domain. Outputs after 100 iterations: (e) difference between (a) and (g) with the S/N value; (f) residual between (b) and reblended data of (g) with its value; (g) and (h) deblended data each in the CS and CR domain.*

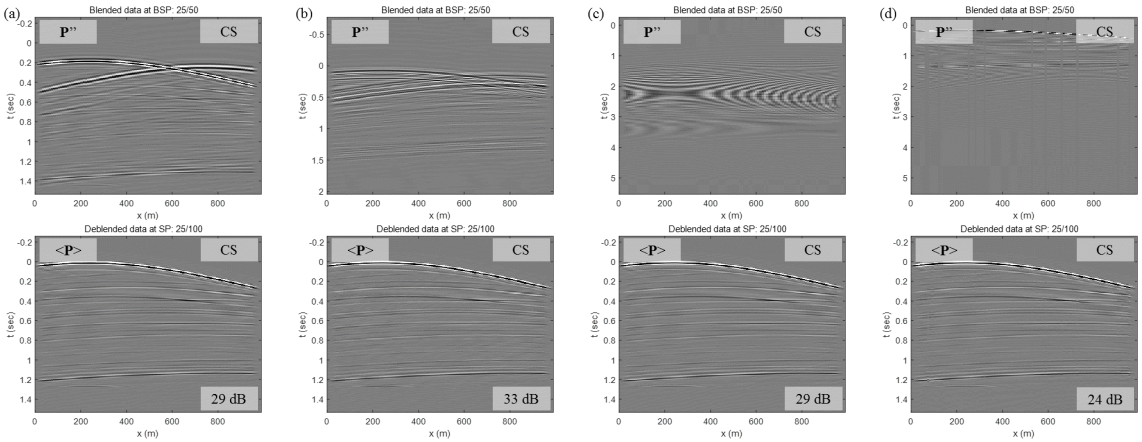

Figure 3 *Results for the blending scenarios 2 to 5: (a) scenario 2 of marine DSA case; (b) scenario 3 of marine popcorn-shooting case; (c) scenario 4 of land DSA case; (d) scenario 5 of a fully generalized case of TZ DSA in addition to non-uniform and under sampling. Blended data at the top and deblended-data after 100 iterations with the S/N value at the bottom. See Figure 2(a) for comparison with the unblended data. The blended wavefields shot by: for (a), (c) and (d), a high-frequency-banded source unit from the left, and a mid from the right; for (d), an airgun unit from the left, and a vibroseis unit from the right, in this particular section.*

Acknowledgements

We thank Adnoc and Inpex Corporation for their supports and permission to publish this paper.

References

Abma, R. and Ross, A. [2013] Popcorn shooting: Sparse inversion and the distribution of airgun array energy over time. *83rd SEG Annual Meeting Technical Program Expanded Abstracts*.

Bagaini, C. [2006] Overview of simultaneous Vibroseis acquisition methods. *76th SEG Annual Meeting Technical Program Expanded Abstracts*.

Berkhout, A. J. [2008] Changing the mindset in seismic data acquisition. *The Leading Edge*, **27**(6), 924–938.

Berkhout, A. J. [2012] Blended acquisition with dispersed source arrays. *Geophysics*, **77**, A19–A23.

Mosher, C. C. [2014] Increasing the efficiency of seismic data acquisition via compressive sensing. *The Leading Edge*, **33**(4), 386-391.